Dictionary-based software for proton dose reconstruction and submilimetric range verification

V.V. Onecha[12], P. Galve[12], P. Ibáñez[12], C. Freijo[12], F. Arias-Valcayo[12], D. Sanchez-Parcerisa[12], S. España[123], L.M. Fraile[12], J.M. Udías[12]

[1] Grupo de Física Nuclear, EMFTEL & IPARCOS, Universidad Complutense de Madrid, CEI Moncloa, Madrid, Spain

[2] Instituto de Investigación Del Hospital Clínico San Carlos (IdISSC), Ciudad Universitaria, Madrid, Spain

[3] Centro Nacional de Investigaciones Cardiovasculares (CNIC), Madrid, Spain

E-mail: vicvalla@ucm.es

Abstract.

Proton therapy are significantly improved if proton range verification techniques are implemented during treatment. They would make it possible to immediately detect deviations in the deposited dose with respect to the plan. Furthermore, they could also provide information to recalculate the plan. The use of PET to verify proton range thanks to the β^+ radiation induced by protons has been studied at length, as the activity produced by these isotopes allows for deriving the proton range. Even, it might be possible to reconstruct the deposited dose from PET activation data, but full dose reconstruction has been scarcely explored. This paper presents a new method that allows for very fast reconstruction, compatible with in-beam use, of both the deposited dose and proton range during proton therapy, using data acquired from a PET scanner. A new MLEM & Simulated Annealing (MSA) algorithm, developed specifically for this work, reconstructs the deposited dose from a realistically pre-calculated activity-dose database (Dictionary). The dictionary contains the activity and dose contribution of each beam in the plan calculated by a Monte Carlo (MC) simulation. The MSA algorithm, using a priori information of the treatment plan, seeks for the linear combination of activities of the precomputed beams that best fits the PET data, obtaining at the same time the deposited dose. The method has been validated with realistic simulations under different situations, determining the minimum dose necessary to reconstruct accurately the deposited dose. A study has also been made of the feasibility of using this method on-line and/or intra-fraction, or with offline inter-fraction verification protocols. Finally, the ability to verify range-shifts induced by deviations with regards to the planning CT has been studied. A realistic proton therapy plan composed of 928 beams of between 120 and 190 MeV generated with matRad from a prostate CT, paired with a clinical commercial PET scanner, was used to carry out these studies. The results show the ability of the method to accurately reconstruct doses from PET data corresponding to activations right after 1 Gy irradiations, both in an intra-fracton and an inter-fraction verification

scenario. For a dose of 1 Gy it has also been shown that the program is able to identify deviations as small as 0.6 mm.

1. Introduction

Proton therapy presents dosimetric advantages over conventional radiotherapy with lighter ionizing particles, such as photons and electrons [1, 2]. These advantages are related to the way the protons deposit their energy, concentrating a significant part of it at the end of their path, and generating a dose peak known as Bragg peak (BP). However, proton therapy is more sensitive to anatomical variations than conventional radiotherapy, as inaccuracies in proton range positioning can lead to severe target underdosage or overdosage of critical structures [1, 3]. Inaccurate conversion of linear attenuation coefficients used in CT scans to stopping power values, errors in patient positioning or alignment, or intrafractional anatomical changes may all be sources of uncertainty of in-patient proton range [1, 3, 4, 5, 6, 7]. The current strategy to mitigate the aforementioned range uncertainties is to extend the target volume by about 3% of the proton range [3, 8, 9, 10] which in turn results in added integral dose to healthy tissues, limiting the potential sparing impact of proton therapy [1]. *In-vivo* proton range verification techniques are being pursued to potentially reduce damage to healthy tissue and increase the benefits of proton therapy.

Most explored solutions for *in-vivo* PT range verification are based on Positron Emission Tomography (PET) [11, 12, 13, 14]. PET-systems are able to detect β^+ isotopes generated by protons in the irradiated regions, and activation maps can be correlated to dose deposition maps [14, 15]. In human tissues, some positron emitters are created by protons at clinical energies via nuclear reactions, mostly ^{15}O and ^{11}C isotopes [16]. Alternatively, PET emitters may be generated by proton interaction with administered contrast agents [17, 18]. The main challenge of *in-vivo* PET dose verification for proton therapy is the derivation of accurate dose maps from experimentally measured activity maps [1, 3, 19] due to the fact that activation and dose are related to different physical processes [12, 14]. Indeed, in the few clinical implementations of PET proton range verification [13, 20], usually dose maps are not derived from activity maps, but measured activity maps were directly compared with planned activity maps derived from Monte Carlo simulations. Any reported deviations were used to flag potential inaccuracies in dose delivery caused by range uncertainties. While this approach can indeed detect range errors with relative success [13, 20], it lacks the ability to perform a full reconstruction of the delivered dose maps, which would in turn allow for online plan adaptations that could make up for any observed under/overdosage. Further, the involvement of lengthy Monte Carlo simulations and the relatively small activation expected, makes it difficult to reconstruct the dose anywhere near to real time.

This issue has been studied extensively in previous works. The first proposed method (and the only one fully implemented in a clinical case), was the *filtering approach* analytical method [21]. This method used the *Pencil Beam* (PB) approximation [22] to transform PET activation maps to absorbed dose maps. The main idea of this method is to fit the observed activity maps to analytical expressions describing proton transport (based on the PB approximation) and nuclear activation processes in order to transform the activity PET images in dose. Fit parameters are precalculated, allowing dose reconstruction to be completed in just a few seconds after the PET image is available. But the principal drawback of this method is the use of approximate analytical expressions for dose calculation, making it significantly less accurate than a Monte Carlo-based approach. An experimental validation of this method was performed by [23] using homogeneous phantoms. Monte Carlo (MC) simulations were also employed to evaluate the accuracy in the reconstruction of dose for treatments based on clinical CT [24]. The results of these validations indicate a precision of 2 mm in proton range estimation, and better than 10% local dose reconstruction. An inconvenient of this method is that it is highly sensitive to the noise in a PET image associated to a 2-Gy irradiation. Other recent works have proposed machine-learning algorithms, in particular recurrent neural networks, for correlating PET activity and proton dose [25, 26]. A recent theoretical study [25] showed a prospective accuracy better than 1 mm in proton range estimation, which is very promising, but the method has implemented only in 1D.

In this work we propose a novel 3D dose reconstruction method using the full power of Monte Carlo simulations [27, 28], but decoupling the time-demanding simulation steps from the reconstruction phase, allowing thus to implemented the method near real-time. This takes advantage of the fact that the vast majority of future and recent proton therapy centers employ active beam scanning.

To this end, a database (or dictionary) of precalculated activity and dose maps for every proton pencil beam in the treatment plan is created, during the planification step. This can be done in a few hours, in a, powerful but otherwise common, computer. During the reconstruction phase, the linear combination of precomputed activity maps from the dictionary which best matches the observed activity is identified, which takes just a few seconds and thus can be performed for intra-fraction verification.

A similar approach has been successfully implemented for protoacoustic range verification [29], also employing a precomputed database, what we call Dose-Activity Dictionary (DAD). Generating the DAD is a time-consuming process, but as said before, in a clinical setting, it could be carried out in parallel to treatment planning, as soon as the simulation CT is available and before the first treatment fraction is delivered. This precalculation step separates realistic simulation of expected activation in a patient CT (using Monte Carlo transport codes) from dose reconstruction, dramatically reducing the amount of time required for the latter. Our algorithm, when fed with a measured PET activity map, uses the existing DAD to find a linear combination of pencil beams that fits the observed PET image. Then, the same linear combination of spots is used to derive the most probable absorbed dose map, a process that takes only a few seconds.

This method has several advantages. The first and most important one the increased accuracy of Monte Carlo calculation (over analytical methods), which is implemented in the DAD calculation. Another benefit is the use of activity maps for individual pencil beams which, combined with precalculation of dose kernels, can help flag problematic areas within the patient volume which may have received a significantly different dose than in the treatment plan.

The main objective of this work is to demonstrate the viability of the proposed method in a clinical setting, focusing on the dependence of the quality of the reconstructed dose maps with two main limiting factors: deposited dose and time interval from dose deposition and PET measurement. Both factors effect directly the PET image quality and therefore, the quality of the reconstructed dose maps [19].

Our approach has been applied to detect range uncertainties originated from in-patient anatomical variations [4] in a prostate plan, whose expected PET activity was realistically simulated as would be detected by a clinical Siemens mMR PET system [30]. In parallel, a DAD was also created for this case and combining the simulated PET images and the DAD, the deposited doses associated to the PET images were obtained and further analyzed using the proposed method.

2. Methods

The proposed verification workflow begins at treatment planning time and ends with the reconstruction of the absorbed dose from detected PET images, captured shortly after irradiation.

2.1. Workflow

The process can be divided in several steps. 1) Calculation of the Dose-Activity Dictionary (DAD) database, which can be done as soon as the the treatment plan is available, and must be ready before the initial fraction is given. 2) After irradiation, patient is taken to an (in-beam, in-room or off the room) clinical PET scanner. The recorded PET data are analyzed to find the linear combination of precalculated pencil beams from the DAD that can reproduce it more accurately. The convergence of this method is controlled by a χ^2 test, to determine the validity of the final solution. 3) If step 2 is satisfactory, the same linear combination of plan spots is used to reconstruct the delivered dose map, which is compared with the reference dose in order to detect potential delivery errors.

2.2. Creation of the Dose-Activity Dictionary (DAD) database

The Dose-Activity Dictionary (DAD) is created by simulating the propagation of all beamlets in the treatment plan across the patient CT, generating deposited dose and isotope-specific activation maps. The Monte Carlo code TOPAS (TOol for PArticle Simulation) [31] is employed for this purpose. The simulated activities for each isotope

are stored separately in order to be able to recreate PET images at any time interval, correcting for the specific half-life of each beta emitter. The simulated activity volumes are filtered/smoothed to reflect the geometry and detection properties of the specific PET system employed; for most systems, a 3D-Gaussian filter point spread function (PSF) is suitable [13, 32]. The PSF must be determined in advance, and it is specific for each PET system but this procedure is straightforward and needs to be performed only once for a given PET scanner. In our case we modeled the PET scanner in a fast Monte Carlo PET simulation [33] and characterize the actual activity maps which would be obtained from the PET scanner under realistic conditions. Realistic MC simulations [34, 35] combined with reconstruction codes [36] help us reproduce the PET signal under realistic conditions, and the actual image quality obtained by the scanner.

TOPAS is particle transport Monte Carlo tool layered on top of Geant4 [37] and specialized in particle therapy physics. For our study, TOPAS version 3.2 was used, along with with Geant4 version 9.6p02x and default physics modules for electromagnetic and nuclear interactions. The used CTs were segmented in Hounsfield Units and the conversion to density and material composition has been used as proposed by [38]. To obtain the β^+ activation maps, a specific TOPAS scorer was developed based on the yield formula [39], adapted to a MC code (1) [18]:

$$Y(\overline{\mathrm{E}}) = \rho_{at}\sigma(\overline{\mathrm{E}})dx \tag{1}$$

where ρ_{at} is the atomic density, σ is the cross section, dx is the step-length of the particle and $\overline{\mathrm{E}}$ is the mean energy of the particle at each step of the path. This formula calculates the production probability of a specific isotope after each proton step during the simulation. The accumulation of these probabilities in the voxels generates the activation distribution. This method provides results with good statistics using a low number of simulated protons, which reduces the simulation time. The reaction channels and the cross-section data used are provided in Table 1.

Isotope	$T_{1/2}$(min)	Reaction Channel	Threshold Energy (MeV)	CS Integral 100 MeV (barn·MeV)	Reference
^{11}C	20.364(20)	^{12}C(p,X)^{11}C	17.9	6.32	[40, 41]
		^{14}N(p,X)^{11}C	3.1	2.61	[42]
		^{16}O(p,X)^{11}C	23.6	1.26	[43, 42]
^{13}N	9.965(4)	^{14}N(p,X)^{13}N	8.9	1.88	[44, 45]
		^{16}O(p,X)^{13}N	5.5	0.65	[43, 42]
^{15}O	2.037(3)	^{16}O(p,X)^{15}O	14.3	5.44	[43, 44, 46, 47]

Table 1: Physical properties of the most relevant isotopes produced in human tissues during a proton irradiation.

2.3. GPU MLEM & Simulated Annealing (MSA) Algorithm

The GPU MLEM & Simulated Annealing (MSA) Reconstruction Algorithm is used to reconstruct the β^+ activation images obtained by a PET system (and therefore the dose deposition) using the precalculated DAD to find the combination of pencil beams that best fits the recorded PET activation image. The algorithm has been implemented in GPU to increase the calculation speed. For this purpose two different parts were implemented, a maximum likelihood estimation method (MLEM) and a Simulated Annealing (SA) functionality.

- MLEM is an iterative algorithm based on the principle of likelihood maximization for parameter estimation. It has been used in many different optimization problems in physics, biology, economy and others [48, 49]. Generally, the reconstruction of an MLEM starts from a flat image and iterates pixel-by-pixel maximizing the loglikelihood until it finds the maximum likelihood between your image and your data. In this work, instead of reconstructing the activation image pixel-by-pixel we use the coefficients of each beam to find the best solution. In order to do that, the general MLEM equation has been used. This allows us to obtain the linear combination of precalculated beams that maximizes the log-likelihood function [50].

$$c_i^{n+1} = \frac{c_i^n}{\sum_j A_{ij}} \sum_j \frac{A_{ij} \cdot d_j}{\sum_i c_i^n \cdot A_{ij}} \tag{2}$$

  Where:

  - **j** is the pixel index of the ROI image.
  - **i** is the index of each pencil beam of the Dictionary.
  - $\mathbf{c_i^n}$ is the **coefficient** of each beam at iteration n: value that multiplies the associated activation and dose image.
  - $\mathbf{d_j}$ is the **data** input activation.
  - $\mathbf{A_{ij}}$ is the activity stored in the **DAD database**. Every pixel data of the ROI image (j index) of each beam of the Dictionary (i index).

- The Simulated Annealing (SA) is used in combinatorial optimization problems in which it is necessary to find some configuration of parameters $\overline{X} = (X_1, X_2, ..., X_N)$ that minimizes some function f($\overline{X}$) [51]. The SA algorithm randomly varies this parameters and analyzes the result according to some *cost function*, which determine if the new solution is better than the previous one. This process is carried out iteratively using the best solution of the precious step to minimize the *cost function*. Our problem can be described in that way associating the beam coefficient to $\overline{X}$ parameters and using the χ^2 test as cost function.

The MSA algorithm requires an initial solution to begin optimization, in this case, a combination of plan spot coefficients. The final solution is, in general, highly dependant on the choice of initial solution. It is not uncommon to use neutral solutions (as would be, in our case, a uniform coefficient distribution) as initial solution. The

advantage of this approach is to avoid using a priori information, so that the final solution is independent of the choice of initial conditions. However, using this approach slows down the convergence to the best solution. Furthermore, in proton therapy the expected solution is, in general, well known, so this knowledge can be used to speed-up the calculation process without loss of generality. Intermediate coefficient distributions between the uniform case and the canonical (planned) case can also be selected. From here on we will refer to as a priori information or a priori initial beam test distribution to the initial solution that mixes information from the expected solution (initial coefficient beam value 1) and the more general case (initial coefficient beam value 0.5).

Both algorithms (MLEM and SA) are applied consecutively defining each cycle of the iterative process as XX iterations of MLEM, followed by YY iterations of SA. This cycle is repeated until a convergence is reached. The combination of MLEM and SA implies that the χ^2 is minimized, while the log-likelihood function is maximized. This combined optimization process avoids getting stuck in local suboptimal solutions of either algorithm, and performs better than both methods separately.

A figure of merit is needed to determine the quality of the obtained dose/activity maps. The control of the activity reconstruction and the evaluation of its quality is contained in a specific parameter developed for the MSA algorithm, in the for of a normalized χ^2 test.

$$\chi^2 = \frac{1}{B} \sum_i \frac{(A_{i,truth} - A_{i,reco})^2}{A_{i,truth} + C} \tag{3}$$

where i is the index of each pixel, $A_{i,truth}$ is the PET input image data set and $A_{i,reco}$ is the reconstructed data. In addition two normalization constants were included. The C constant depends on the PET input image and its value is equal to a 5% of the maximum activity in the PET image. This is the smaller threshold which eliminates the effect of background noise without affecting the global result. On the other side, the B constant normalises the χ^2 so that the expected solution obtained from the DAD provides a value of χ^2 equal to 1 when it is compared to a simulated PET image that has been calculated from the expected solution.

3. Benchmark Study

An extensive theoretical study has been performed to test the potential of the DAD MSA Algorithm. A clinical proton therapy plan for a prostate CT has been used to study the dose dependence of the method, the viability of different acquisition time intervals for the PET and the ability of the method to identify minimal anatomical changes in the CT. The performance of a Siemens Biograph mMR PET system to detect the induced activity has been simulated in detail. .

3.1. Creation of the dose-activity dictionary

A realistic prostate treatment plan has been generated using matRad [52] covering a target volume defined over prostate CT [53] segmented in 24 biological materials following Schneider et. al [38]. The treatment comprises 927 beams of energies between 130 and 190 MeV. These beams have a Gaussian spatial distribution with sigma values of 0.21 cm and 0.28 cm in Y and Z, respectively.

Therefore, a DAD was created with 927 data sets of dose and activity of ^{15}O, ^{13}N and ^{11}C for each beam. They were generated with TOPAS using 10^5 histories for each beamlet. A volume with 150x60x70 pixels of dimensions 1x2x2 mm^3 (XYZ, with finer grid size in the beam propagation direction) was used as region of interest (ROI). This region includes the whole dose deposited by every pencil beam in the prostate and its vicinity (see Fig 1). The total amount of space required to store the complete dictionary is 9.2 GB and the time required to do that is about 6 hours.

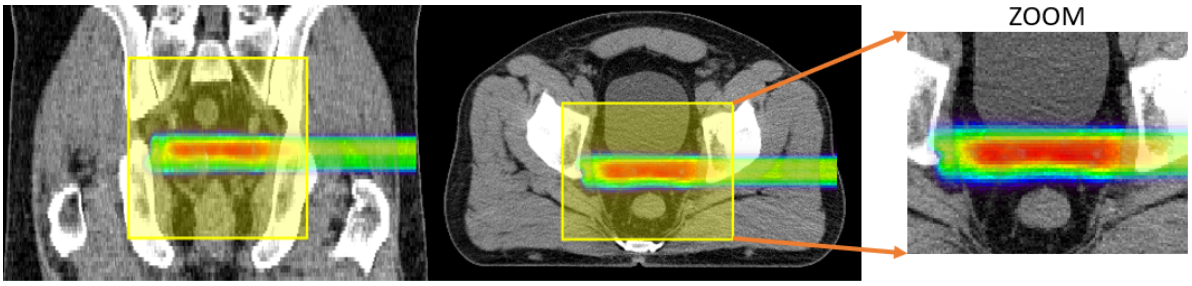

Figure 1: Whole dose contribution as result of the sum of every pencil beam simulated for the Dictionary database. In yellow the region of interest (ROI) where data is stored.

3.2. Simulation of PET images

To generate the PET signal resulting from the proton activation, the Siemens mMR Biograph [30] system was chosen, a state-of-the-art clinical PET scanner. This scanner is composed of 8 rings with 56 detector blocks each, 8x8 lutetium oxyorthosilicate crystals (4x4x20 mm) per block, covering a transverse field of view (FOV) of 59.4 cm and an axial FOV of 25.8 cm. The energy resolution is 14.5% at 511 keV, and the energy window is 430-610 keV. In Figure 2 we show the scheme of the scanner and the human CT used for the study case of this work.

PET signals of the mMR Biograph were simulated using the Ultra-fast MC PET simulator [33], a GPU-accelerated code for MC transport of photons that includes the physics related to positron range, photon interactions with the CT, and detector response. The activities used as input to generate PET signals were generated taking into account the dose deposited and the time interval of the PET measurements. To build the dictionary, high statistical activities were simulated, to avoid contributing to statistical noise. Photon emissions are generated all over the space taking into account the density probabilities provided by the activity distributions. The number of the simulated photons in for each beam is high enough to avoid noise produced by

MC simulations. The simulated PET signal is reconstructed including normalization, resolution modeling with PSF, attenuation, and scatter corrections in the Ordered Subsets Expectation Maximization algorithm with a maximum a priori regularization (MAP-OSEM) [54, 55].

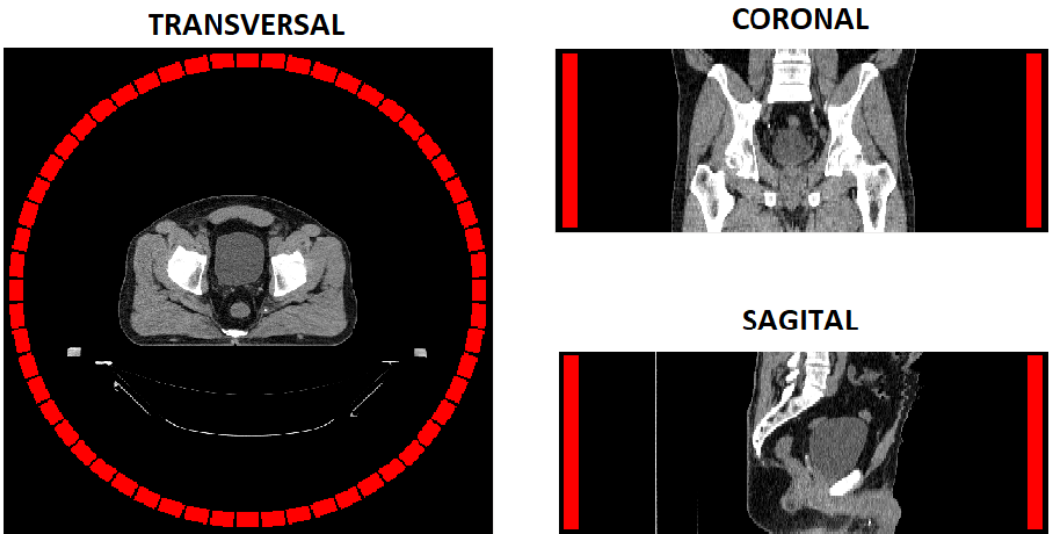

Figure 2: Siemens Biograph mMR system (red) used for the photon simulation by the Ultra-fast Monte Carlo PET simulator [33] to obtain realistic PET signals. The prostate CT chosen to validate the method is represented at the same geometrical position with respect to the PET as it was used to simulate the photon transport.

3.3. Test scenarios

Different scenarios were selected to test the proper functioning of the DAD MSA-Algorithm using the treatment plan and the PET system previously described.

(i) **Quality of reconstructed dose maps according to the dose administered:** absorbed dose is directly related to the number of generated β^+ isotopes, so the quality of the PET image (and therefore, of the reconstructed dose map) depends on it. Using a dictionary proton beam with a range in water of 21 cm, PET images and reconstructed dose maps were generated for doses ranging from 0.01 Gy to 10 Gy. Beyond 10 Gy it was observed that the reconstructed dose does not improve any further.

(ii) **Dependence of image reconstruction quality on the PET data acquisition time:** increasing acquisition time and therefore the statistics of the activation maps also has a positive impact on the quality of the reconstructed dose maps. To study the viability of online vs. offline acquisition, we performed a similar analysis to (i) using all dictionary beams in the 179-180 MeV interval, a fixed dose of 1 Gy and two acquisition scenarios: in-room (0-1 minutes post irradiation) and offline (10-30 minutes post-irradiation).

(iii) **Sensitivity of reconstructed dose to anatomical changes**: in order to mimic realistic clinical situations where interfractional anatomical changes occur, we simulated these changes by altering the density of a certain CT region in the beam path. This produces variations in the proton range which may lead to a final deposited dose different from what was expected [4, 56, 57]. To study the sensitivity of our approach to these variations, we recreated two scenarios. First, a global 10% density increase was considered (CT-Altered-Box), causing a maximum range shift of 8 mm. Second, a 10% density increase was applied to a slice of 1 cm perpendicular to the beam (CT-Altered-Slice), introducing a range shift of just 0.6 mm.

3.4. Metrics

To evaluate the accuracy of the dose reconstruction, we define a set of metrics to compare the reconstructed dose with the reference dose (ground truth), as calculated by TOPAS. These metrics will be combined to flag possible dose deviations due to range errors or interfractional anatomical changes.

(i) Comparison of the derived in-patient ranges R_{90}, R_{50} and R_{10} in reconstructed and planned dose maps. These R# represents the position of the dose along the longitudinal profile where the dose is a #% of the maximum value of the Bragg Peak [5, 58]. "Range deviation" histograms are created by studying the R# values for every pixel in the transversal XY plan, considering all non-zero voxels in the beam propagation direction.

(ii) Pixel-by-pixel dose deviation, calculated as the relative error between the reconstructed and planned dose maps [24], as

$$RE_{Dose} = \frac{D_i - D_{i,ref}}{max_i(D_{i,ref})} \cdot 100, \tag{4}$$

where D_i is the i-th voxel of the reconstructed dose and $D_{i,ref}$ is the i-th voxel of the reference dose.

(iii) Gamma analysis as defined by [59], quantifying agreement between measured and reference dose distributions in terms of both relative dose difference and distance to agreement (DTA). The γ criteria is defined as

$$\gamma(r_m) = min\{\Gamma(r_m, r_c)\}\forall\{r_c\} \tag{5}$$

where Γ is defined as

$$\Gamma(r_m, r_c) = \sqrt{\frac{r^2(r_m, r_c)}{\Delta d_M^2} + \frac{\delta^2(r_m, r_c)}{\Delta D_M^2}} \tag{6}$$

in which a gamma less than 1 indicates a satisfactory result for a specific pixel. For this work the values of Δd_M and ΔD_M were set to 1 mm and 3% of the maximum dose respectively (gamma 1mm-3% with dose global criteria). Only voxels with at least 5% of the maximum dose value where taken into account for the gamma

analysis. Gamma analysis was applied separately to the complete dose image and to the dose fall-off region, to further evaluate the ability of our algorithm for range verification.

4. Results

4.1. Sensitivity to fraction dose

Three different activity maps, associated to respective doses of 0.1, 1 and 10 Gy delivered by a 180-MeV pencil beam, were simulated and further reconstructed (as described in Section 2). No a priori information was used for dose reconstruction, i.e. a uniform distribution of beams was used as initial solution. Simulated activity maps and reconstructed dose distribution are shown in Fig 3, with dose profiles detailed in Fig. 4. Dose curves reconstructed with above 1 Gy are virtually indistinguishable from reference dose; for lower dose (0.1 Gy), reconstructed dose (normalized to maximum) is locally overestimated by 5% along the beam profile, contributing to the RE_{DOSE} with values close to 2% (fig 5d) because of the normalization applied in this parameter. Furthermore, the reconstructed range is about 2 mm shorter than the reference case.

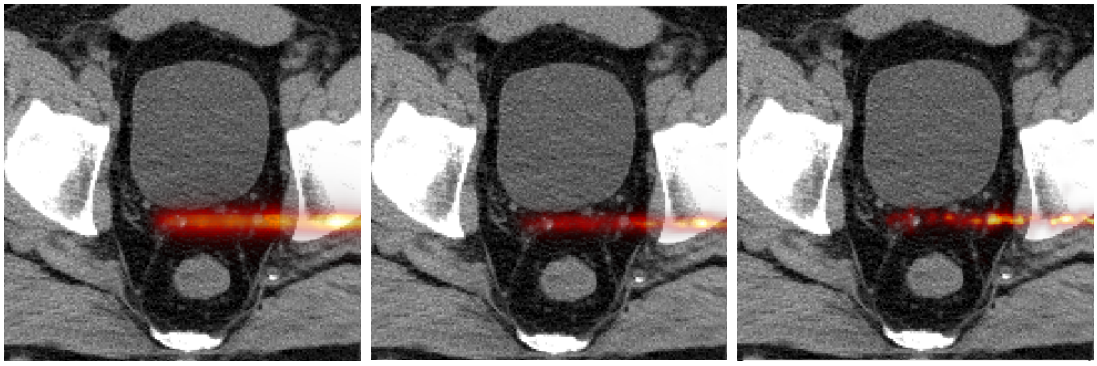

(a) PET Activity - 10 Gy (b) PET Activity - 1 Gy (c) PET Activity - 0.1 Gy

(d) Dose - 10 Gy (e) Dose - 1 Gy (f) Dose - 0.1 Gy

Figure 3: (a-c) Simulated PET activities, associated to 0.1, 1 and 10 Gy, used as input for the dose reconstruction. (d-f) Reconstructed doses from each of the PET activities.

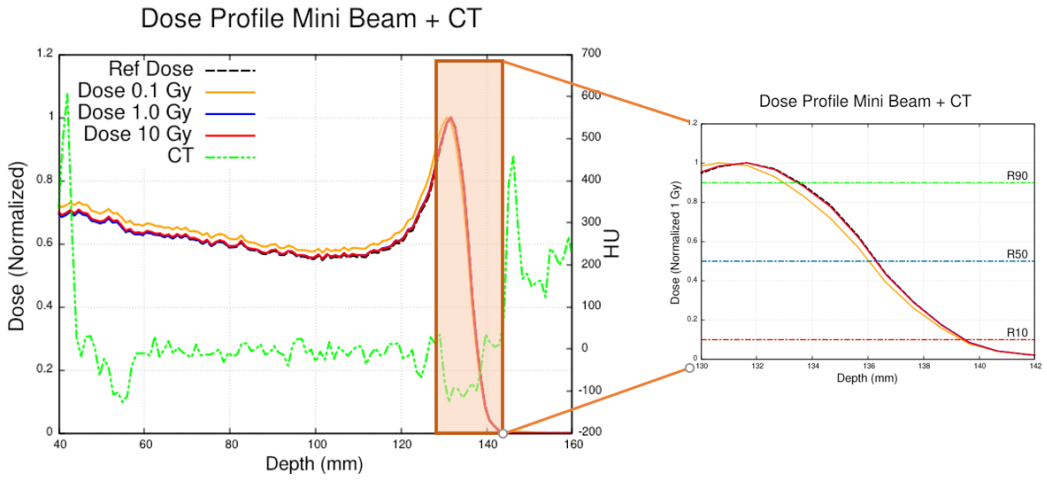

Figure 4: Central dose profiles representation of the reconstructed doses from PET activities associated to 10, 1 and 0.1 Gy and the ground truth dose (Ref dose). A zoom of the fall-off of the Bragg peak (orange box) is also represented.

To further quantify the obtained differences, range and dose deviation (the latter named RE_{DOSE}) histograms of each of the three reconstructed doses were calculated (Fig. 5) and also its mean and sigma values were obtained (Table 2). In this table also the 1mm-3% gamma test results are shown. The results are coherent with the observed the dose profiles. Values of RE_{DOSE} close to zero indicate a practically perfect reconstruction of the dose (within 1%) in every case. In terms of range, for 10 and 1 Gy, no deviations above 0.2 mm are observed in any of the considered pixels. However, for the lowest dose of 0.1 Gy, range errors of up to 1 mm are observed, which are highest for R_{90} and decrease the further away from the BP. Furthermore, the gamma test analysis shows a perfect dose reconstruction in the 10 and 1 Gy examples (pass rate above 99.99%) but decreases to 95.62 for the 0.1-Gy test.

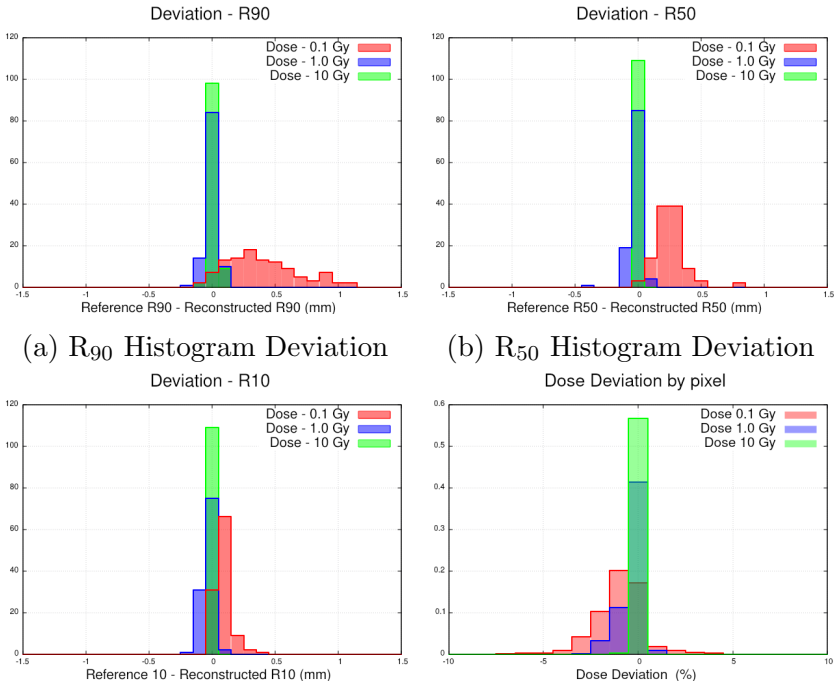

(a) R_{90} Histogram Deviation (b) R_{50} Histogram Deviation

(c) R_{10} Histogram Deviation (d) Dose Histogram Deviation

Figure 5: Range deviation histograms of the R_{90}, R_{50} and R_{10} (a-c) and Dose Deviation histogram (d). The histograms show the results for doses of 0.1, 1.0 and 10 Gy (red, blue and green, respectively).

Dose (Gy)	R_{90} (mm)		R_{50} (mm)		R_{10} (mm)		RE_{DOSE} (%)		Gamma Analysis
	Mean	σ	Mean	σ	Mean	σ	Mean	σ	1mm-3%
10	0.01	0.03	0.00	0.00	0.00	0.00	0.00	0.07	100
1	0.00	0.05	-0.02	0.06	-0.03	0.05	-0.32	0.61	99.99
0.1	0.43	0.37	0.25	0.12	0.09	0.07	-0.94	1.32	95.62

Table 2: Mean and sigma values of range and dose deviation histograms of the reconstructed pencil beam doses in Fig. 5

4.2. Sensitivity to acquisition modality

Two different activation maps associated to a dose of 1 Gy and two different acquisition schemes were studied: in-room PET (simulated by measuring interval 0-1 min post irradiation) and offline PET (10-30 min after irradiation). Both schemes were simulated and used to obtain reconstructed dose maps using the algorithm described in Section 2. Reference dose and activation maps obtained from the Monte Carlo code are shown in

Fig 6, together with reconstructed activation and dose maps. Initially, reconstructions were carried out starting from a homogeneous distribution of beam coefficients.

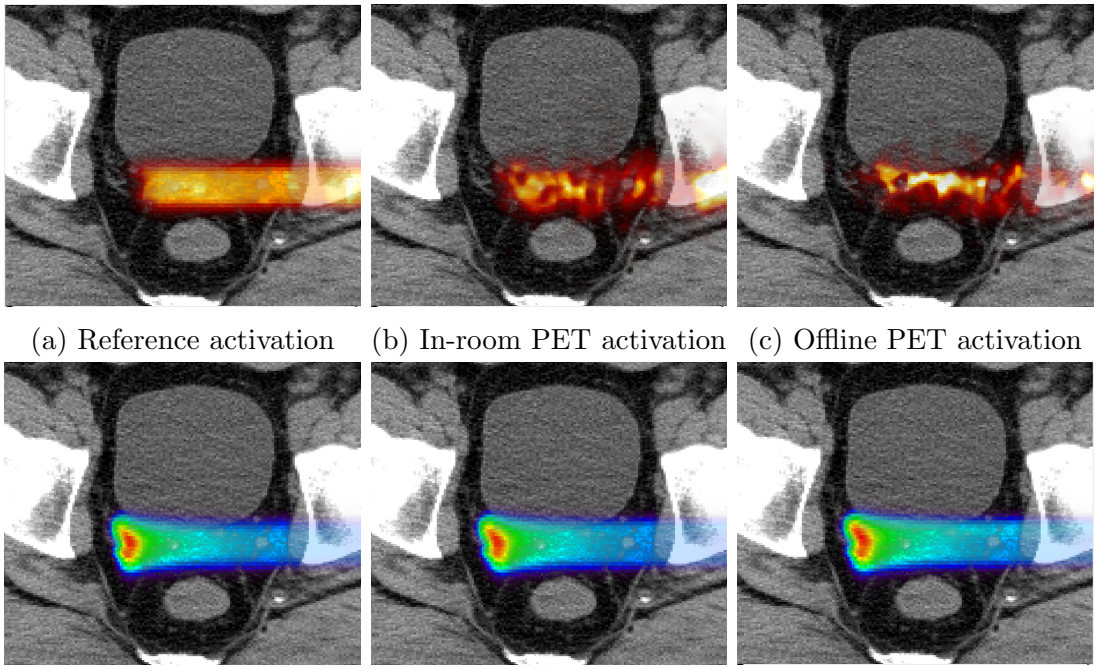

(a) Reference activation (b) In-room PET activation (c) Offline PET activation

(d) Reference dose (e) In-room dose (f) Offline dose

Figure 6: Reference dose and activation produced by TOPAS of the distal dose (a,d). Reconstructed dose and simulated PET image associated with the 0-1 min time interval after the irradiation (b,e) and the 10-30 time interval (c,f).

Range and relative dose deviation histograms can be seen in Fig 7. Mean and sigma values of the associated distributions are shown in Table 3. Note that the integrated activity is about 2 times higher in the offline scheme than in the in-room scheme (see table 3). At the view of this data, two effects can be spotted in the reconstruction. First, reconstructed doses tend to be slightly blurred compared to the reference dose distributions, which in turn results in a positive shift of the observed Bragg peak and R_{90} values and an overall slight underestimation of the local dose. In terms of dose deviation, the results are satisfactory since in both cases 90% of the pixels suffer a deviation below 5% compared to the reference dose. These effect is caused by an overestimation of the coefficients associated to low-dose beams, as seen in the RE_{DOSE} histogram in Fig 7d. The blurring presents similar trends for both in-room and offline acquisition.

Second, the dispersion in the calculated ranges seen in the in-room study (about 4-5 times larger than in the offline study) implies that reconstructing a PET image associated to a dose of 1 Gy with a 1-minute acquisition is not suitable, at least using a uniform distribution of coefficients as input.

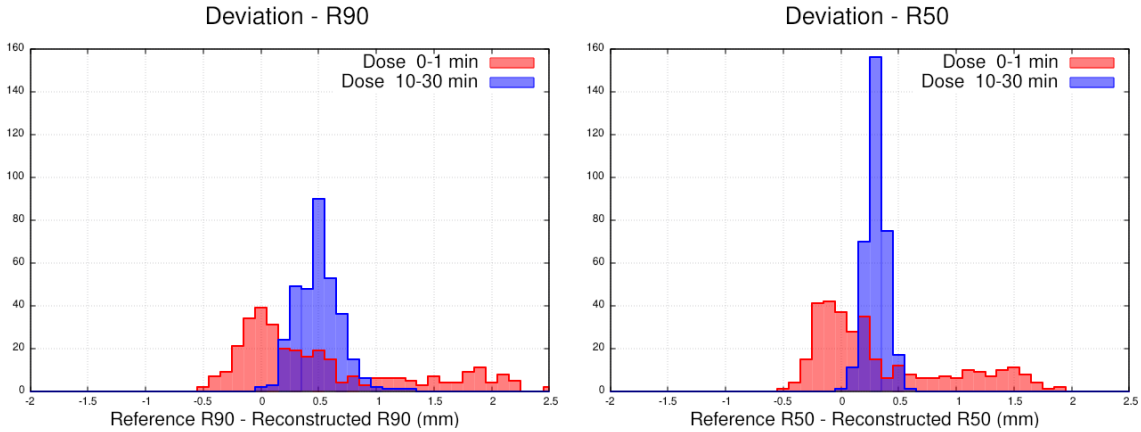

(a) R_{90} Deviation (b) R_{50} Deviation

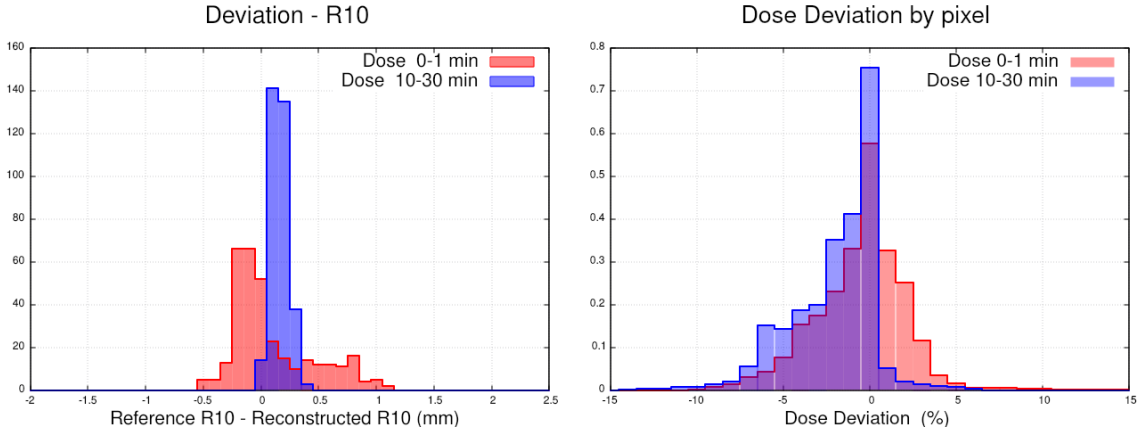

(c) R_{10} Deviation (d) Dose Deviation

Figure 7: Range (R_{90}, R_{50} and R_{10}) and dose deviation histograms for each acquisition modality: in-room (0-1 min, red) and offline (10-30 min, blue).

Time (min)	Decays	Dose (Gy)	R_{90} (mm)		R_{50} (mm)		R_{10} (mm)		RE_{DOSE}(%)	
		Mean	σ	Mean	σ	Mean	σ	Mean	σ	
0 - 1	$6.3{\cdot}10^5$	1	0.54	0.77	0.35	0.59	0.09	0.35	-0.64	2.71
10 - 30	$1.19{\cdot}10^6$	1	0.49	0.19	0.31	0.09	0.16	0.08	-1.96	2.45

Table 3: Mean and sigma values of range and dose deviations histograms of the reconstructed distal doses in Fig. 7.

To improve this result, we repeated the study using the planned distribution of beam coefficients as initial solution for the reconstruction algorithm. The results (Table 4) show a substantial improvement in the obtained dose maps in comparison with the uniform (more general) case. Using this methodology, we observe that the reconstruction artifacts seen previously are solved: blurring is reduced to a minimum and ranges can be

reproduced with submillimetric precision for both acquisition modalities, in-room and offline. The use of the planned distribution of beam coefficients as input clearly improves the quality of the reconstructed dose. However, using this a priori information might, in principle, imply a lost of generality and hamper dose reconstruction if anatomical changes are present. Precisely, in the next section we explore the ability of the DAD-MSA algorithm using a priori information to detect anatomical changes in planning CT and reconstruct absorbed dose in modified patient geometries.

Dose 1.0 Gy - Planned Beam Distribution as Input

Time Interval (min)	Dose (Gy)	R_{90} (mm)		R_{50} (mm)		R_{10} (mm)		RE_{DOSE}(%)	
		Mean	σ	Mean	σ	Mean	σ	Mean	σ
0 - 1	1.0	0.08	0.42	0.09	0.47	-0.16	0.48	-0.62	2.21
10 - 30	1.0	0.04	0.36	0.12	0.52	0.09	0.32	-0.35	1.23

Table 4: Mean and sigma values of range deviations histograms of Distal Activation associated to 1.0 Gy reconstructed using the expected distribution of coefficients as input condition.

4.3. Detection of anatomical variations in planning CT

Fig 8 shows reconstructed dose maps for the three study cases, namely reference case, altered box (10% global density increase, causing a shift of 8 mm) and altered-slice (10% density increase in a 1-cm slice, causing a shift of 0.6 mm). Reconstructions were performed using a priori information from treatment plan as initial solution for the inverse problem. A dose of 1 Gy in the target volume was used for all case and an offline scheme was applied.

The results of the study, in the form of associated range deviation histograms, statistics of the distributions and gamma analysis, are presented in Fig 9 and Table 5.

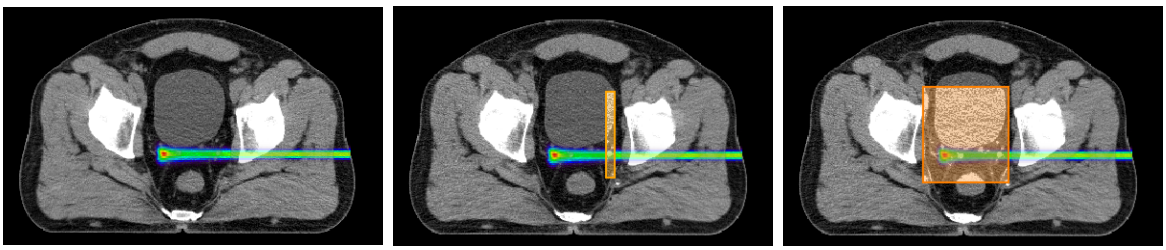

(a) Original CT (b) Slice Altered CT (c) Box Altered CT

Figure 8: Reconstructed dose overlying planning CTs for the three cases under study. The altered regions with a density increment of a 10% are remarked in orange.

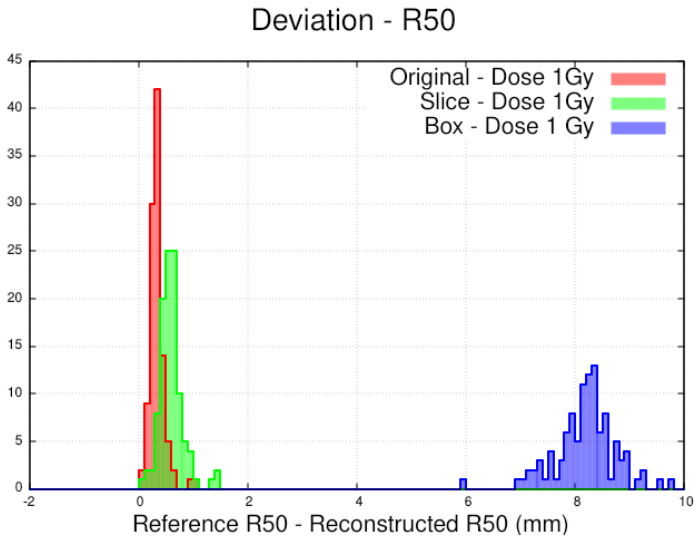

Figure 9: R_{50} deviation histogram with respect to reference dose for original CT (red), slice-altered CT (green) and box-altered CT (blue).

Case	R_{50} (mm)		Expected	Gamma 1mm-3%	
	Mean	σ	R_{50} (mm)	Total	Fall-off
Original CT	0.13	0.14	0.00	93.99	92.40
Slice CT	0.55	0.22	0.61	83.20	84.24
Box CT	8.14	0.56	8.03	72.33	5.87

Table 5: Statistics of the range deviation histograms (Fig. 9) and gamma analysis

Results show that both metrics under study (range deviation and gamma analysis) can potentially be used to detect range shifts as small as 0.6 mm caused by anatomical variations in the planning CT using the MSA algorithm, provided that relevant thresholds are defined.

The analysis of R_{50} from the reconstructed distributions for slice- and box-altered CTs can be easily used to detect range variations. The mean value (calculated as the average range shift over all voxels in the XY plane irradiated by the beamlet) is compatible with the expected range shift induced by the CT density modification.

Finally, the gamma analysis test can also be used to flag inadequate dose depositions, particularly if applied to a certain area of interest near the distal edge of the planned dose distribution. While more than 70% of the considered voxels can still pass the test even with an 8-mm global range shift (box CT), this number is decreased to only 5% of the "fall-off" voxels, providing a clear way of identifying failed irradiations. Again, this number is reduced from 92% to 84% for the 0.6-mm shift (slice CT), which

suggests that appropriate thresholds can be found to flag potential delivery errors in reconstructed activity patterns.

5. Discussion

A novel workflow for proton dose reconstruction from PET activation is proposed, as an alternative to the existing ones such as the *filtering approach* [21] and the use of deep learning [25, 60]. It is based on a Dose-Activity Dictionary (DAD) database and a GPU implementation of the MLEM & Simulated Annealing (MSA) algorithm that reconstructs dose maps from acquired PET images. The developed DAD-MSA software is natively three-dimensional and it can be adapted to any clinical scenario (beam pulse, PET time measurement, etc.). By construction, it produces inherently noiseless dose distributions, which represents a clear advantage over others [24, 60] and simplifies analyzing range distributions and identifying potential delivery errors.

In view of the presented dose-dependency study, we expect our method to be able of accurately reconstructing doses larger or equal than 1 Gy. For specific (simpler) situations, such as the reconstruction of an individual pencil beam, dose can be reconstructed with remarkable agreement from the activation obtained after just a 0.1 Gy irradiation.

The DAD-MSA algorithm could, in principle, be applied to both *in-room* and *off-line* PET proton range verification schemes. While the offline approach (with higher integrated activity, but which may suffer from biological wash-out [32, 61, 62, 63, 64]) presents slightly better results, both schemes have been proven viable for dose reconstruction, provided that a priori information from treatment planning is used as an input to the reconstruction algorithm.

These numbers represent a breakthrough in comparison with previous works [24, 60], which required doses of about 2-6 Gy and time intervals of 10-15 minutes after irradiation, significantly higher than the 1-Gy dose and first-minute reconstruction used in this work, yet achieving comparable accuracy.

Our implementation of the DAD-MSA algorithm using a priori information from treatment planning has proven effective at detecting anatomical variations in a realistic clinical scenario resulting in altered dose distributions [3, 4, 8]. We were able to effectively detect range shifts smaller than 1 mm, for a deposited dose comparable to a treatment fraction (1 Gy) and offline acquisition. Furthermore, the ability to perform a full dose reconstruction in an instantaneous fashion allows us to perform a deeper analysis on the absorbed dose distribution, such as gamma-analysis (Table 5), which would allow the treatment team to establish realistic thresholds for intra-fraction replanning, and to decide on potential plan adaptations for subsequent sessions to make up for delivery errors.

From a technical point of view, there is some room for improvement in certain aspects of the dose reconstruction algorithm, which we leave for future works. We have observed a tendency of the DAD-MSA algorithm to overestimate the flat dose region

proximal to the Bragg peak, causing a slight underestimation of the relative proton range. This is caused by activity in this region being erroneously attributed to low-energy beams rather than higher-energy beams: the MSA algorithm fails to establish a zero-contribution for the former, which causes a smoothing of the coefficients which translates into a smoothing of the dose distribution, broadening the Bragg peak. On the contrary, high-energy beams tend to be avoided, as any activity contribution beyond the limit of the PET images is strongly penalized in the calculation of the χ^2. A potential improvement on the method would have to consider this effect, adding a correction factor to the χ^2 value used in the optimization to avoid over-penalizing high-energy beams. Moreover, the biological *wash-out* effect [32, 61, 62, 63, 64] (i.e. diffusion of β^+ isotopes in patient body after irradiation) has not been included in our study yet. While probably negligible for the online and in-room approaches, its effect should be studied in detail for offline acquisition by implementing a time-dependent version of the Ultra-fast MC PET simulator, encapsulating PET machine dependence and patient washout.

6. Conclusions

We propose a novel method to reconstruct maps of deposited dose in proton therapy from measured PET secondary radiation in an instantaneous fashion. Our software is able to reconstruct doses from 1 Gy for both online and offline approaches by using a priori information of the treatment plan and patient anatomy. The algorithm also presents a favorable response at detecting anatomical variations causing submillimetric variations in the in-patient range. Experimental tests of the proposed method are now required to validate the observed findings.

References

[1] Knopf, Antje C. ; Lomax, Antony: In vivo proton range verification: A review. In: Physics in Medicine and Biology 58 (2013), Nr. 15, S. 131–160. http://dx.doi.org/10.1088/0031-9155/58/15/R131. – DOI 10.1088/0031–9155/58/15/R131. – ISBN 1361–6560

[2] Hoskin, Peter J. ; Bhattacharya, Indrani S.: Protons and more: state of the art in radiotherapy. In: Clinical medicine (London, England) 14 (2014), dec, Nr. Suppl 6, s61–s65. http://dx.doi.org/10.7861/clinmedicine.14-6-s61. – DOI 10.7861/clinmedicine.14–6–s61. – ISSN 14734893

[3] Paganetti, Harald: Range uncertainties in proton therapy and the role of Monte Carlo simulations. In: Physics in Medicine and Biology 57 (2012), jun, Nr. 11, R99–R117. http://dx.doi.org/10.1088/0031-9155/57/11/R99. – DOI 10.1088/0031–9155/57/11/R99. – ISBN 0031–9155

[4] Lomax, A. J.: Intensity modulated proton therapy and its sensitivity to treatment uncertainties 1: The potential effects of calculational uncertainties. In: Physics in Medicine and Biology 53 (2008), feb, Nr. 4, 1027–1042. http://dx.doi.org/10.1088/0031-9155/53/4/014. – DOI 10.1088/0031–9155/53/4/014. – ISSN 00319155

[5] Schuemann, J ; Dowdell, S ; Grassberger, C ; Min, C H. ; Paganetti, H: Site-specific range uncertainties caused by dose calculation algorithms for proton therapy. In: Physics in Medicine and Biology 59 (2014), aug, Nr. 15, 4007–4031. http://dx.doi.org/10.1088/0031-9155/59/15/4007. – DOI 10.1088/0031–9155/59/15/4007. – ISSN 0031–9155

[6] España, Samuel ; Paganetti, Harald: The impact of uncertainties in the CT conversion algorithm when predicting proton beam ranges in patients from dose and PET-activity distributions. In: Physics in Medicine and Biology 55 (2010), dec, Nr. 24, 7557–7571. http://dx.doi.org/10.1088/0031-9155/55/24/011. – DOI 10.1088/0031–9155/55/24/011. – ISSN 0031–9155

[7] Palta, Jatinder ; Yeung, Daniel: Precision and Uncertainties in Proton Therapy for Nonmoving Targets. Version: dec 2011. http://dx.doi.org/10.1201/b11448-14. 2011. – DOI 10.1201/b11448–14, 413–434

[8] Carabe, Alejandro ; Moteabbed, Maryam ; Depauw, Nicolas ; Schuemann, Jan ; Paganetti, Harald: Range uncertainty in proton therapy due to variable biological effectiveness. In: Physics in Medicine and Biology 57 (2012), mar, Nr. 5, 1159–1172. http://dx.doi.org/10.1088/0031-9155/57/5/1159. – DOI 10.1088/0031–9155/57/5/1159. – ISSN 0031–9155

[9] Seco, Joao ; Gu, Guan ; Marcelos, Tiago ; Kooy, Hanne ; Willers, Henning: Proton arc reduces range uncertainty effects and improves conformality compared with photon volumetric modulated arc therapy in stereotactic body radiation therapy for non-small cell lung cancer. In: International Journal of Radiation

Oncology Biology Physics 87 (2013), sep, Nr. 1, S. 188–194. http://dx.doi.org/10.1016/j.ijrobp.2013.04.048. – DOI 10.1016/j.ijrobp.2013.04.048. – ISSN 03603016

[10] Liu, Wei ; Zhang, Xiaodong ; Li, Yupeng ; Mohan, Radhe: Robust optimization of intensity modulated proton therapy. In: Medical Physics 39 (2012), feb, Nr. 2, 1079–1091. http://dx.doi.org/10.1118/1.3679340. – DOI 10.1118/1.3679340. – ISSN 00942405

[11] Parodi, Katia: Latest developments in in-vivo imaging for proton therapy. In: The British Journal of Radiology 93 (2020), mar, Nr. 1107, 20190787. http://dx.doi.org/10.1259/bjr.20190787. – DOI 10.1259/bjr.20190787. – ISSN 0007–1285

[12] Parodi, K. ; Ponisch, F. ; Enghardt, W.: Experimental study on the feasibility of in-beam PET for accurate monitoring of proton therapy. In: IEEE Transactions on Nuclear Science 52 (2005), jun, Nr. 3, 778–786. http://dx.doi.org/10.1109/TNS.2005.850950. – DOI 10.1109/TNS.2005.850950. – ISSN 0018–9499

[13] Zhu, Xuping ; España, Samuel ; Daartz, Juliane ; Liebsch, Norbert ; Ouyang, Jinsong ; Paganetti, Harald ; Bortfeld, Thomas R. ; El Fakhri, Georges: Monitoring proton radiation therapy with in-room PET imaging. In: Physics in Medicine and Biology 56 (2011), jul, Nr. 13, 4041–4057. http://dx.doi.org/10.1088/0031-9155/56/13/019. – DOI 10.1088/0031–9155/56/13/019. – ISSN 0031–9155

[14] Paganetti, H. ; Fakhri, G. E.: Monitoring proton therapy with PET. In: British Journal of Radiology 88 (2015), jul, Nr. 1051, 20150173. http://dx.doi.org/10.1259/bjr.20150173. – DOI 10.1259/bjr.20150173. – ISSN 00071285

[15] Zhu, Xuping ; El Fakhri, Georges: Proton therapy verification with PET imaging. In: Theranostics 3 (2013), sep, Nr. 10, 731–740. http://dx.doi.org/10.7150/thno.5162. – DOI 10.7150/thno.5162. – ISBN 1838–7640 (Electronic) 1838–7640 (Linking)

[16] España, S. ; Zhu, X. ; Daartz, J. ; El Fakhri, G. ; Bortfeld, T. ; Paganetti, H.: The reliability of proton-nuclear interaction cross-section data to predict proton-induced PET images in proton therapy. In: Physics in Medicine and Biology 56 (2011), may, Nr. 9, 2687–2698. http://dx.doi.org/10.1088/0031-9155/56/9/003. – DOI 10.1088/0031–9155/56/9/003. – ISBN 0031–9155

[17] Espinosa, A. ; Onecha, V.V. ; Sánchez-Tembleque, V. ; Gutiérrez-Neira, C. ; García-Díez, M. ; Ibáñez, P. ; España, S. ; Sánchez-Parcerisa, D. ; Udías, J.M. ; Fraile, L.M.: Can iodine be used as a contrast agent for protontherapy range verification? Measurement of the 127I(p,n)127mXe (reaction) cross section in the 4.5-10 MeV energy range. In: Radiation Physics and Chemistry 185 (2021), aug, S. 109485. http://dx.doi.org/10.1016/j.radphyschem.2021.109485. – DOI 10.1016/j.radphyschem.2021.109485. – ISSN 0969806X

[18] España, Samuel ; Sánchez-Parcerisa, Daniel ; Ibáñez, Paula ; Sánchez-Tembleque, Víctor ; Udías, Jose M. ; Onecha, V ; Gutierrez-Uzquiza, Alvaro ; Bäcker, Claus M. ; Bäumer, Christian ; Herrmann, Ken ; Fragoso Costa, Pedro ; Timmermann, Beate ; Fraile, Luis M.: Direct proton range verification using oxygen-18 enriched water as a contrast agent. In: Radiation Physics and Chemistry 182 (2021), 109385. http://dx.doi.org/10.1016/j.radphyschem.2021.109385. – DOI 10.1016/j.radphyschem.2021.109385

[19] Parodi, Katia ; Polf, Jerimy C.: ¡i¿In vivo¡/i¿ range verification in particle therapy. In: Medical Physics 45 (2018), nov, Nr. 11, e1036–e1050. http://dx.doi.org/10.1002/mp.12960. – DOI 10.1002/mp.12960. – ISSN 0094–2405

[20] Parodi, K. ; Bauer, J. ; Kurz, C. ; Unholtz, D. ; Sommerer, F. ; Frey, K. ; Haberer, T. ; Herfarth, K. ; Welzel, T. ; Combs, S. ; Debus, J.: WE-G-500-06: Offline PET/CT Imaging of Scanned Proton and Carbon Ion Beams: Initial Clinical Experience for Different Tumour Sites. In: Medical Physics Bd. 40, John Wiley and Sons, Ltd, jun 2013. – ISSN 00942405, 504

[21] Parodi, Katia ; Bortfeld, Thomas: A filtering approach based on Gaussian–powerlaw convolutions for local PET verification of proton radiotherapy. In: Physics in Medicine and Biology 51 (2006), apr, Nr. 8, 1991–2009. http://dx.doi.org/10.1088/0031-9155/51/8/003. – DOI 10.1088/0031–9155/51/8/003. – ISSN 0031–9155

[22] Hong, Linda ; Goitein, Michael ; Bucciolini, Marta ; Comiskey, Robert ; Gottschalk, Bernard ; Rosenthal, Skip ; Serago, Chris ; Urie, Marcia: A pencil beam algorithm for proton dose calculations. In: Physics in Medicine and Biology 41 (1996), aug, Nr. 8, 1305–1330. http://dx.doi.org/10.1088/0031-9155/41/8/005. – DOI 10.1088/0031–9155/41/8/005. – ISBN 0031–9155

[23] Masuda, Takamitsu ; Nishio, Teiji ; Kataoka, Jun ; Arimoto, Makoto ; Sano, Akira ; Karasawa, Kumiko: ML-EM algorithm for dose estimation using PET in proton therapy. In: Physics in Medicine and Biology 64 (2019), sep, Nr. 17, 175011. http://dx.doi.org/10.1088/1361-6560/ab3276. – DOI 10.1088/1361–6560/ab3276. – ISSN 1361–6560

[24] Masuda, Takamitsu ; Nishio, Teiji ; Sano, Akira ; Karasawa, Kumiko: Extension of the ML-EM algorithm for dose estimation using PET in proton therapy: Application to an inhomogeneous target. In: Physics in Medicine and Biology 65 (2020), jun, Nr. 18. http://dx.doi.org/10.1088/1361-6560/ab98cf. – DOI 10.1088/1361–6560/ab98cf. – ISSN 13616560

[25] Liu, Chuang ; Li, Zhongxing ; Hu, Wenbin ; Xing, Lei ; Peng, Hao: Range and dose verification in proton therapy using proton-induced positron emitters and recurrent neural networks (RNNs). In: Physics in Medicine and Biology 64 (2019), sep, Nr. 17, 175009. http://dx.doi.org/10.1088/1361-6560/ab3564. – DOI 10.1088/1361–6560/ab3564. – ISSN 1361–6560

[26] Li, Zhongxing ; Wang, Yiang ; Yu, Yajun ; Fan, Kuanjun ; Xing, Lei ; Peng, Hao: Technical Note: Machine learning approaches for range and dose verification in proton therapy using proton-induced positron emitters. In: Medical Physics 46 (2019), dec, Nr. 12, 5748–5757. http://dx.doi.org/10.1002/mp.13827. – DOI 10.1002/mp.13827. – ISSN 00942405

[27] Paganetti, H. ; Jiang, H. ; Lee, S. Y. ; Kooy, H. M.: Accurate Monte Carlo simulations for nozzle design, commissioning and quality assurance for a proton radiation therapy facility. In: Medical Physics 31 (2004), jul, Nr. 7, 2107–2118. http://dx.doi.org/10.1118/1.1762792. – DOI 10.1118/1.1762792. – ISSN 00942405

[28] Mairani, A ; Böhlen, T T. ; Schiavi, A ; Tessonnier, T ; Molinelli, S ; Brons, S ; Battistoni, G ; Parodi, K ; Patera, V: A Monte Carlo-based treatment planning tool for proton therapy. In: Physics in Medicine and Biology 58 (2013), apr, Nr. 8, 2471–2490. http://dx.doi.org/10.1088/0031-9155/58/8/2471. – DOI 10.1088/0031–9155/58/8/2471. – ISSN 0031–9155

[29] Freijo, Clara ; Herraiz, Joaquin L. ; Sanchez-Parcerisa, Daniel ; Udias, José Manuel: Dictionary-based protoacoustic dose map imaging for proton range verification. In: Photoacoustics 21 (2021), mar, S. 100240. http://dx.doi.org/10.1016/j.pacs.2021.100240. – DOI 10.1016/j.pacs.2021.100240. – ISSN 22135979

[30] Delso, Gaspar ; Fürst, Sebastian ; Jakoby, Björn ; Ladebeck, Ralf ; Ganter, Carl ; Nekolla, Stephan G. ; Schwaiger, Markus ; Ziegler, Sibylle I.: Performance measurements of the siemens mMR integrated whole-body PET/MR scanner. In: Journal of Nuclear Medicine 52 (2011), dec, Nr. 12, 1914–1922. http://dx.doi.org/10.2967/jnumed.111.092726. – DOI 10.2967/jnumed.111.092726. – ISSN 01615505

[31] Perl, J. ; Shin, J. ; Schümann, J. ; Faddegon, B. ; Paganetti, H.: TOPAS: An innovative proton Monte Carlo platform for research and clinical applications. In: Medical Physics 39 (2012), Nr. 11, S. 6818–6837. http://dx.doi.org/10.1118/1.4758060. – DOI 10.1118/1.4758060. – ISSN 00942405

[32] Parodi, Katia ; Paganetti, Harald ; Shih, Helen A. ; Michaud, Susan ; Loeffler, Jay S. ; DeLaney, Thomas F. ; Liebsch, Norbert J. ; Munzenrider, John E. ; Fischman, Alan J. ; Knopf, Antje ; Bortfeld, Thomas: Patient Study of In Vivo Verification of Beam Delivery and Range, Using Positron Emission Tomography and Computed Tomography Imaging After Proton Therapy. In: International Journal of Radiation Oncology Biology Physics 68 (2007), jul, Nr. 3, 920–934. http://dx.doi.org/10.1016/j.ijrobp.2007.01.063. – DOI 10.1016/j.ijrobp.2007.01.063. – ISBN 0360–3016

[33] Galve, Pablo ; Arias-Valcayo, Fernando ; Lopez-Montes, Alejandro ; Villa-Abaunza, A. ; Ibanez, Paula ; Herraiz, Joaquin L. ; Udias, Jose M.: Multi-

purpose Ultra-fast Monte Carlo PET simulator. In: 2020 IEEE Nuclear Science Symposium and Medical Imaging Conference Proceedings (NSS/MIC), 2020

[34] Abushab, K. M. ; Herraiz, J. L. ; Vicente, E. ; Cal-Gonzalez, J. ; Espana, S. ; Vaquero, J. J. ; Jakoby, B. W. ; Udias, J. M.: Evaluation of PeneloPET Simulations of Biograph PET/CT Scanners. In: IEEE Transactions on Nuclear Science 63 (2016), jun, Nr. 3, 1367–1374. http://dx.doi.org/10.1109/TNS.2016.2527789. – DOI 10.1109/TNS.2016.2527789. – ISBN 0018–9499 VO – 63

[35] Lopez-Montes, Alejandro ; Herraiz, Joaquin L. ; Galve, Pablo ; Espana, Samuel ; Vicente, Esther ; Cal-Gonzalez, Jacobo ; Udias, Jose M.: PeneloPET v3.0, an improved multiplatform PET Simulator. In: 2019 IEEE Nuclear Science Symposium and Medical Imaging Conference (NSS/MIC), IEEE, oct 2019. – ISBN 978–1–7281–4164–0, 1–3

[36] Galve, Pablo ; Herraiz, Joaquin L. ; Catana, Ciprian ; Udias, Jose M.: GPU based Fast and Flexible Iterative Reconstructions of Arbitrary and Complex PET Scanners: Application to Next Generation Dedicated Brain Scanners. In: 2020 IEEE Nuclear Science Symposium and Medical Imaging Conference Proceedings (NSS/MIC), 2020

[37] Agostinelli, S. ; Allison, J. ; Amako, K. ; Apostolakis, J. ; Araujo, H. ; Arce, P. ; Asai, M. ; Axen, D. ; Banerjee, S. ; Barrand, G. ; Behner, F. ; Bellagamba, L. ; Boudreau, J. ; Broglia, L. ; Brunengo, A. ; Burkhardt, H. ; Chauvie, S. ; Chuma, J. ; Chytracek, R. ; Cooperman, G. ; Cosmo, G. ; Degtyarenko, P. ; Dell'Acqua, A. ; Depaola, G. ; Dietrich, D. ; Enami, R. ; Feliciello, A. ; Ferguson, C. ; Fesefeldt, H. ; Folger, G. ; Foppiano, F. ; Forti, A. ; Garelli, S. ; Giani, S. ; Giannitrapani, R. ; Gibin, D. ; Gomez Cadenas, J. J. ; Gonzalez, I. ; Gracia Abril, G. ; Greeniaus, G. ; Greiner, W. ; Grichine, V. ; Grossheim, A. ; Guatelli, S. ; Gumplinger, P. ; Hamatsu, R. ; Hashimoto, K. ; Hasui, H. ; Heikkinen, A. ; Howard, A. ; Ivanchenko, V. ; Johnson, A. ; Jones, F. W. ; Kallenbach, J. ; Kanaya, N. ; Kawabata, M. ; Kawabata, Y. ; Kawaguti, M. ; Kelner, S. ; Kent, P. ; Kimura, A. ; Kodama, T. ; Kokoulin, R. ; Kossov, M. ; Kurashige, H. ; Lamanna, E. ; Lampen, T. ; Lara, V. ; Lefebure, V. ; Lei, F. ; Liendl, M. ; Lockman, W. ; Longo, F. ; Magni, S. ; Maire, M. ; Medernach, E. ; Minamimoto, K. ; Mora de Freitas, P. ; Morita, Y. ; Murakami, K. ; Nagamatu, M. ; Nartallo, R. ; Nieminen, P. ; Nishimura, T. ; Ohtsubo, K. ; Okamura, M. ; O'Neale, S. ; Oohata, Y. ; Paech, K. ; Perl, J. ; Pfeiffer, A. ; Pia, M. G. ; Ranjard, F. ; Rybin, A. ; Sadilov, S. ; Salvo, E. di ; Santin, G. ; Sasaki, T. ; Savvas, N. ; Sawada, Y. ; Scherer, S. ; Sei, S. ; Sirotenko, V. ; Smith, D. ; Starkov, N. ; Stoecker, H. ; Sulkimo, J. ; Takahata, M. ; Tanaka, S. ; Tcherniaev, E. ; Safai Tehrani, E. ; Tropeano, M. ; Truscott, P. ; Uno, H. ; Urban, L. ; Urban, P. ; Verderi, M. ; Walkden, A. ; Wander, W.

; Weber, H. ; Wellisch, J. P. ; Wenaus, T. ; Williams, D. C. ; Wright, D. ; Yamada, T. ; Yoshida, H. ; Zschiesche, D.: GEANT4 - A simulation toolkit. In: Nuclear Instruments and Methods in Physics Research, Section A: Accelerators, Spectrometers, Detectors and Associated Equipment (2003). http://dx.doi.org/10.1016/S0168-9002(03)01368-8. – DOI 10.1016/S0168–9002(03)01368–8. – ISSN 01689002

[38] Schneider, Wilfried ; Bortfeld, Thomas ; Schlegel, Wolfgang: Correlation between CT numbers and tissue parameters needed for Monte Carlo simulations of clinical dose distributions. In: Physics in Medicine and Biology 45 (2000), feb, Nr. 2, S. 459–478. http://dx.doi.org/10.1088/0031-9155/45/2/314. – DOI 10.1088/0031–9155/45/2/314. – ISSN 00319155

[39] Krasnov, N.N.: Thick target yield. In: International Journal of Applied Radiation and Isotopes 25 (1974), Nr. 5, 223–227. https://inis.iaea.org/search/search.aspx?orig_q=RN:5133688

[40] Measday, David F.: The 12C(p, pn)11C reaction from 50 to 160 MeV. In: Nuclear Physics 78 (1966), apr, Nr. 2, S. 476–480. http://dx.doi.org/10.1016/0029-5582(66)90621-3. – DOI 10.1016/0029–5582(66)90621–3. – ISSN 00295582

[41] Whitehead, A. B. ; Foster, J. S.: ACTIVATION CROSS SECTIONS FOR C ^{12} (p , pn)C ^{11} , O ^{16} (p , α)N ^{13} , and F ^{19} (p , pn)F ^{18}. In: Canadian Journal of Physics 36 (1958), oct, Nr. 10, 1276–1285. http://dx.doi.org/10.1139/p58-132. – DOI 10.1139/p58–132. – ISSN 0008–4204

[42] Takács, S. ; Tárkányi, F. ; Hermanne, A. ; Paviotti de Corcuera, R.: Validation and upgrading of the recommended cross section data of charged particle reactions used for production of PET radioisotopes. In: Nuclear Instruments and Methods in Physics Research, Section B: Beam Interactions with Materials and Atoms 211 (2003), oct, Nr. 2, S. 169–189. http://dx.doi.org/10.1016/S0168-583X(03)01264-3. – DOI 10.1016/S0168–583X(03)01264–3. – ISSN 0168583X

[43] Masuda, Takamitsu ; Kataoka, Jun ; Arimoto, Makoto ; Takabe, Miho ; Nishio, Teiji ; Matsushita, Keiichiro ; Miyake, Tasuku ; Yamamoto, Seiichi ; Inaniwa, Taku ; Toshito, Toshiyuki: Measurement of nuclear reaction cross sections by using Cherenkov radiation toward high-precision proton therapy. In: Scientific Reports 8 (2018), dec, Nr. 1, S. 1–8. http://dx.doi.org/10.1038/s41598-018-20906-z. – DOI 10.1038/s41598–018–20906–z. – ISSN 20452322

[44] Sajjad, M. ; Lambrecht, R. M. ; Wolf, A. P.: Cyclotron Isotopes and Radiopharmaceuticals: XXXVI Investigation of Some Excitation Functions for the Preparation of 15O, 13N and 11C. In: Radiochimica Acta 38 (1985), jan, Nr. 2, 57–64. http://dx.doi.org/10.1524/ract.1985.38.2.57. – DOI 10.1524/ract.1985.38.2.57. – ISSN 21933405

[45] Hess, E. ; Scholten, B. ; Coenen, H. H. ; Qaim, S. M. ; Takács, S. ; Tárkányi, F.: Excitation function of the 18O(p,n)18F nuclear reaction

from threshold up to 30 MeV. In: Radiochimica Acta 89 (2001), jun, Nr. 37043, S. 357. http://dx.doi.org/10.1524/ract.2001.89.6.357. – DOI 10.1524/ract.2001.89.6.357. – ISSN 00338230

[46] Valentin, L.: Réactions (p, n) et (p, pn) Induites à moyenne énergie sur des noyaux légers. In: Nuclear Physics 62 (1965), feb, Nr. 1, S. 81–102. http://dx.doi.org/10.1016/0029-5582(65)90072-6. – DOI 10.1016/0029–5582(65)90072–6. – ISSN 00295582

[47] Akagi, T. ; Yagi, M. ; Yamashita, T. ; Murakami, M. ; Yamakawa, Y. ; Kitamura, K. ; Ogura, K. ; Kondo, K. ; Kawanishi, S.: Experimental study for the production cross sections of positron emitters induced from 12C and 16O nuclei by low-energy proton beams. In: Radiation Measurements 59 (2013), dec, S. 262–269. http://dx.doi.org/10.1016/j.radmeas.2013.07.005. – DOI 10.1016/j.radmeas.2013.07.005. – ISSN 13504487

[48] Maxim, Voichita ; Lojacono, Xavier ; Hilaire, Estelle ; Krimmer, Jochen ; Testa, Etienne ; Dauvergne, Denis ; Magnin, Isabelle ; Prost, Rémy: Probabilistic models and numerical calculation of system matrix and sensitivity in list-mode MLEM 3D reconstruction of Compton camera images. In: Physics in Medicine and Biology 61 (2016), jan, Nr. 1, 243–264. http://dx.doi.org/10.1088/0031-9155/61/1/243. – DOI 10.1088/0031–9155/61/1/243. – ISSN 0031–9155

[49] Ma, Dan ; Wolf, Paul ; Clough, Anne V. ; Schmidt, Taly G.: The performance of MLEM for dynamic imaging from simulated few-view, multi-pinhole SPECT. In: IEEE Transactions on Nuclear Science 60 (2013), Nr. 1, 115–123. http://dx.doi.org/10.1109/TNS.2012.2214235. – DOI 10.1109/TNS.2012.2214235. – ISSN 00189499

[50] Shepp, L. A. ; Vardi, Y.: Maximum Likelihood Reconstruction for Emission Tomography. In: IEEE Transactions on Medical Imaging 1 (1982), Nr. 2, S. 113–122. http://dx.doi.org/10.1109/TMI.1982.4307558. – DOI 10.1109/TMI.1982.4307558. – ISSN 1558254X

[51] Rutenbar, Rob A.: Simulated annealing algorithms: An overview. In: IEEE Circuits and Devices Magazine 5 (1989), jan, Nr. 1, S. 19–26. http://dx.doi.org/10.1109/101.17235. – DOI 10.1109/101.17235. – ISSN 87553996

[52] Wieser, Hans P. ; Cisternas, Eduardo ; Wahl, Niklas ; Ulrich, Silke ; Stadler, Alexander ; Mescher, Henning ; Muller, Lucas R. ; Klinge, Thomas ; Gabrys, Hubert ; Burigo, Lucas ; Mairani, Andrea ; Ecker, Swantje ; Ackermann, Benjamin ; Ellerbrock, Malte ; Parodi, Katia ; Jakel, Oliver ; Bangert, Mark: Development of the open-source dose calculation and optimization toolkit matRad. In: Medical Physics 44 (2017), jun, Nr. 6, 2556–2568. http://dx.doi.org/10.1002/mp.12251. – DOI 10.1002/mp.12251. – ISSN 00942405

[53] Craft, David ; Bangert, Mark ; Long, Troy ; Papp, Dávid ; Unkelbach, Jan: Shared data for intensity modulated radiation therapy (IMRT) optimization research: The CORT dataset. In: GigaScience 3 (2014), dec, Nr. 1. http://dx.doi.org/10.1186/2047-217X-3-37. – DOI 10.1186/2047–217X–3–37. – ISSN 2047217X

[54] Hudson, H. M. ; Larkin, Richard S.: Accelerated Image Reconstruction Using Ordered Subsets of Projection Data. In: IEEE Transactions on Medical Imaging 13 (1994), Nr. 4, S. 601–609. http://dx.doi.org/10.1109/42.363108. – DOI 10.1109/42.363108. – ISSN 1558254X

[55] Bettinardi, V. ; Pagani, E. ; Gilardi, M. ; Alenius, S. ; Thielemans, K. ; Teras, M. ; Fazio, F.: Implementation and evaluation of a 3D one-step late reconstruction algorithm for 3D positron emission tomography brain studies using median root prior. In: European Journal of Nuclear Medicine 29 (2002), apr, Nr. 1, 7–18. http://dx.doi.org/10.1007/s002590100651. – DOI 10.1007/s002590100651. – ISSN 03406997

[56] Hui, Zhouguang ; Zhang, Xiaodong ; Starkschall, George ; Li, Yupeng ; Mohan, Radhe ; Komaki, Ritsuko ; Cox, James D. ; Chang, Joe Y.: Effects of Interfractional Motion and Anatomic Changes on Proton Therapy Dose Distribution in Lung Cancer. In: International Journal of Radiation Oncology Biology Physics 72 (2008), dec, Nr. 5, 1385–1395. http://dx.doi.org/10.1016/j.ijrobp.2008.03.007. – DOI 10.1016/j.ijrobp.2008.03.007. – ISSN 03603016

[57] Yang, Zhiyong ; Zhang, Xiaodong ; Wang, Xianliang ; Zhu, X. R. ; Gunn, Brandon ; Frank, Steven J. ; Chang, Yu ; Li, Qin ; Yang, Kunyu ; Wu, Gang ; Liao, Li ; Li, Yupeng ; Chen, Mei ; Li, Heng: Multiple-CT optimization: An adaptive optimization method to account for anatomical changes in intensity-modulated proton therapy for head and neck cancers. In: Radiotherapy and Oncology 142 (2020), jan, 124–132. http://dx.doi.org/10.1016/j.radonc.2019.09.010. – DOI 10.1016/j.radonc.2019.09.010. – ISSN 18790887

[58] Tommasino, F. ; Rovituso, M. ; Fabiano, S. ; Piffer, S. ; Manea, C. ; Lorentini, S. ; Lanzone, S. ; Wang, Z. ; Pasini, M. ; Burger, W. J. ; La Tessa, C. ; Scifoni, E. ; Schwarz, M. ; Durante, M.: Proton beam characterization in the experimental room of the Trento Proton Therapy facility. In: Nuclear Instruments and Methods in Physics Research, Section A: Accelerators, Spectrometers, Detectors and Associated Equipment 869 (2017), oct, S. 15–20. http://dx.doi.org/10.1016/j.nima.2017.06.017. – DOI 10.1016/j.nima.2017.06.017. – ISSN 01689002

[59] Low, Daniel A. ; Harms, William B. ; Mutic, Sasa ; Purdy, James A.: A technique for the quantitative evaluation of dose distributions. Version: 1998. http://dx.doi.org/10.1118/1.598248. 1998. – Forschungsbericht

[60] Ma, Saiqun ; Hu, Zongsheng ; Ye, Kuangkuang ; Zhang, Xiaoke ; Wang, Yuenan ; Peng, Hao: Feasibility study of patient-specific dose verification

in proton therapy utilizing positron emission tomography (PET) and generative adversarial network (GAN). In: Medical Physics 47 (2020), aug, Nr. 10, 5194–5208. http://dx.doi.org/10.1002/mp.14443. – DOI 10.1002/mp.14443. – ISSN 00942405

[61] Ammar, C ; Frey, K ; Bauer, J ; Melzig, C ; Chiblak, S ; Hildebrandt, M ; Unholtz, D ; Kurz, C ; Brons, S ; Debus, J ; Abdollahi, A ; Parodi, K: Comparing the biological washout of β^+ -activity induced in mice brain after ^{12} C-ion and proton irradiation. In: Physics in Medicine and Biology 59 (2014), dec, Nr. 23, 7229–7244. http://dx.doi.org/10.1088/0031-9155/59/23/7229. – DOI 10.1088/0031–9155/59/23/7229. – ISBN 0031–9155

[62] Bauer, Julia ; Chen, Wenjing ; Nischwitz, Sebastian ; Liebl, Jakob ; Rieken, Stefan ; Welzel, Thomas ; Debus, Juergen ; Parodi, Katia: Improving the modelling of irradiation-induced brain activation for in vivo PET verification of proton therapy. In: Radiotherapy and Oncology 128 (2018), jul, Nr. 1, S. 101–108. http://dx.doi.org/10.1016/j.radonc.2018.01.016. – DOI 10.1016/j.radonc.2018.01.016. – ISSN 18790887

[63] Toramatsu, Chie ; Yoshida, Eiji ; Wakizaka, Hidekazu ; Mohammadi, Akram ; Ikoma, Yoko ; Tashima, Hideaki ; Nishikido, Fumihiko ; Kitagawa, Atsushi ; Karasawa, Kumiko ; Hirano, Yoshiyuki ; Yamaya, Taiga: Washout effect in rabbit brain: in-beam PET measurements using ^{10}C, ^{11}C and ^{15}O ion beams. In: Biomedical Physics and Engineering Express 4 (2018), mar, Nr. 3, 035001. http://dx.doi.org/10.1088/2057-1976/aaade7. – DOI 10.1088/2057–1976/aaade7. – ISSN 2057–1976

[64] Mizuno, H ; Tomitani, T ; Kanazawa, M ; Kitagawa, A ; Pawelke, J ; Iseki, Y ; Urakabe, E ; Suda, M ; Kawano, A ; Iritani, R ; Matsushita, S ; Inaniwa, T ; Nishio, T ; Furukawa, S ; Ando, K ; Nakamura, Y K. ; Kanai, T ; Ishii, K: Washout measurement of radioisotope implanted by radioactive beams in the rabbit. In: Physics in Medicine and Biology 48 (2003), aug, Nr. 15, 2269–2281. http://dx.doi.org/10.1088/0031-9155/48/15/302. – DOI 10.1088/0031–9155/48/15/302. – ISSN 0031–9155